

Supporting Information

Towards the self-assembly of metal-organic
nanotubes using metal-metal and π -stacking
interactions: Bis(pyridylethynyl) silver(I)
metallomacrocycles and coordination polymers.

*Kelly J. Kilpin,^a Martin L. Gower,^a Geoffrey B. Jameson,^b Shane G. Telfer,^{b,c} and
James D. Crowley*^a*

^aDepartment of Chemistry, University of Otago, PO Box 56, Dunedin,

New Zealand; Fax: +64 3 479 7906; Tel: +64 3 479 7731.

^bInstitute of Fundamental Sciences, Massey University, Private Bag 11 222, Palmerston North, New
Zealand.

^cMacDiarmid Institute for Advanced Materials and Nanotechnology, New Zealand.

* jcrowley@chemistry.otago.ac.nz

TABLE OF CONTENTS

1.	Molecular Modelling	S3
2.	Selected NMR Spectra of the Ligands and Stacked Plots	S4
3.	Selected HR ESI-MS of the Au(I) complexes	S9
4.	Selected NMR Spectra and Stacked Plots of the Ag(I) complexes	S10
5.	Selected HR ESI-MS of the Ag(I) complexes	S12
6.	Proposed Structures of the MSPMs	S15
7.	X-ray Crystallography	S16
7.1	Packing Diagrams for $[(L_3)_2Ag_2](ClO_4)_2 \cdot 3H_2O$	S16
7.2	Packing Diagrams for $\{[L_5Ag](ClO_4) \bullet 0.5Et_2O\}_n$	S19
7.3	Packing Diagrams for $\{[L_3Ag](SbF_6)_2\}_n$	S20
8.	X-ray Crystallographic Data	S22

1. Molecular Modeling

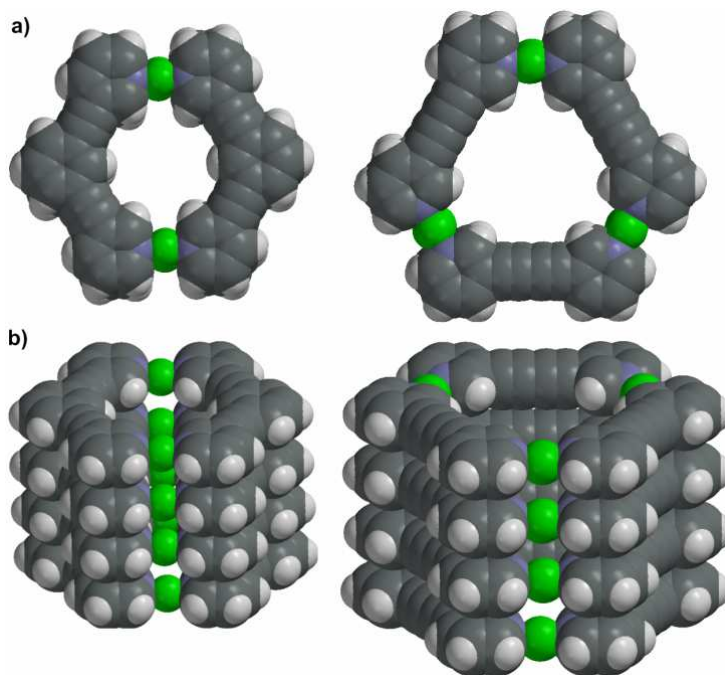


Figure S1: A space-filling representation of the proposed metal organic nanotubes potentially formed through the stacking of silver(I) or gold(I) planar MSPMs. This cartoon was generated using Spartan '06 Essential Edition for Windows, Wavefunction, Irvine, CA.

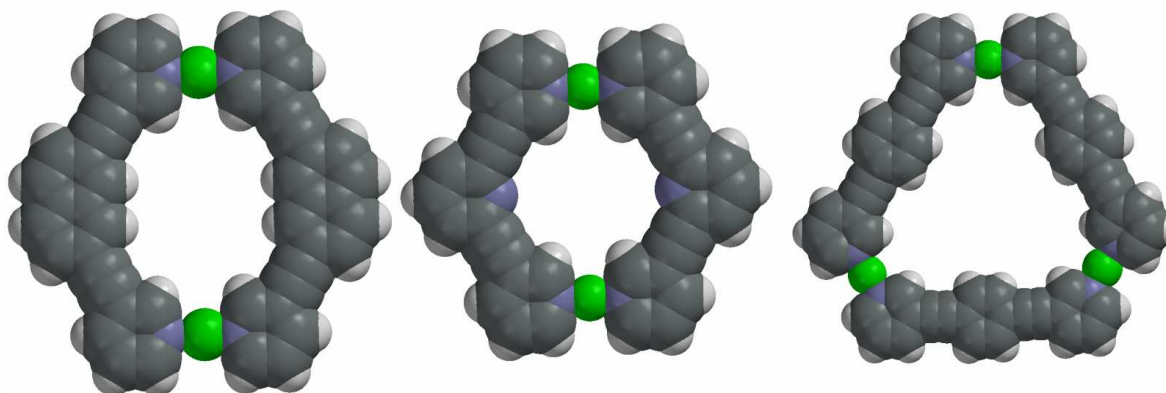


Figure S2: Space-filling molecular models of the proposed solution structures of $[(L_4)_2Ag_2](SbF_6)_2$ (left), $[(L_5)_2Ag_2](SbF_6)_2$ (center) and $[(L_2)_3Ag_3](SbF_6)_3$ (right). The counter anions are omitted for clarity. These cartoons were generated using Spartan '06 Essential Edition for Windows, Wavefunction, Irvine, CA.

2. Selected NMR Spectra and Stacked Plots

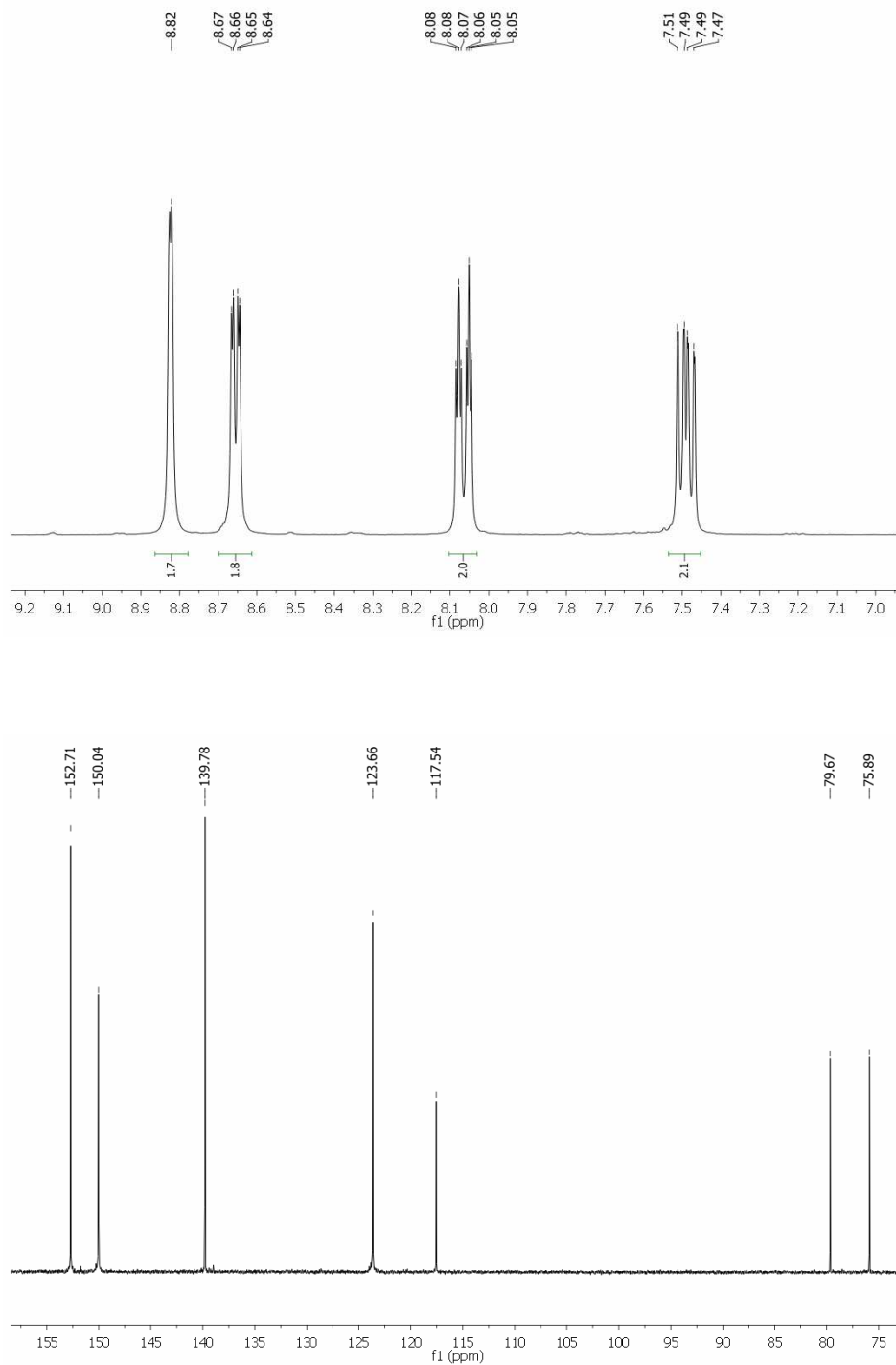


Figure S3: ^1H (top) and ^{13}C (bottom) NMR spectra (d_6 -DMSO) of **L1**

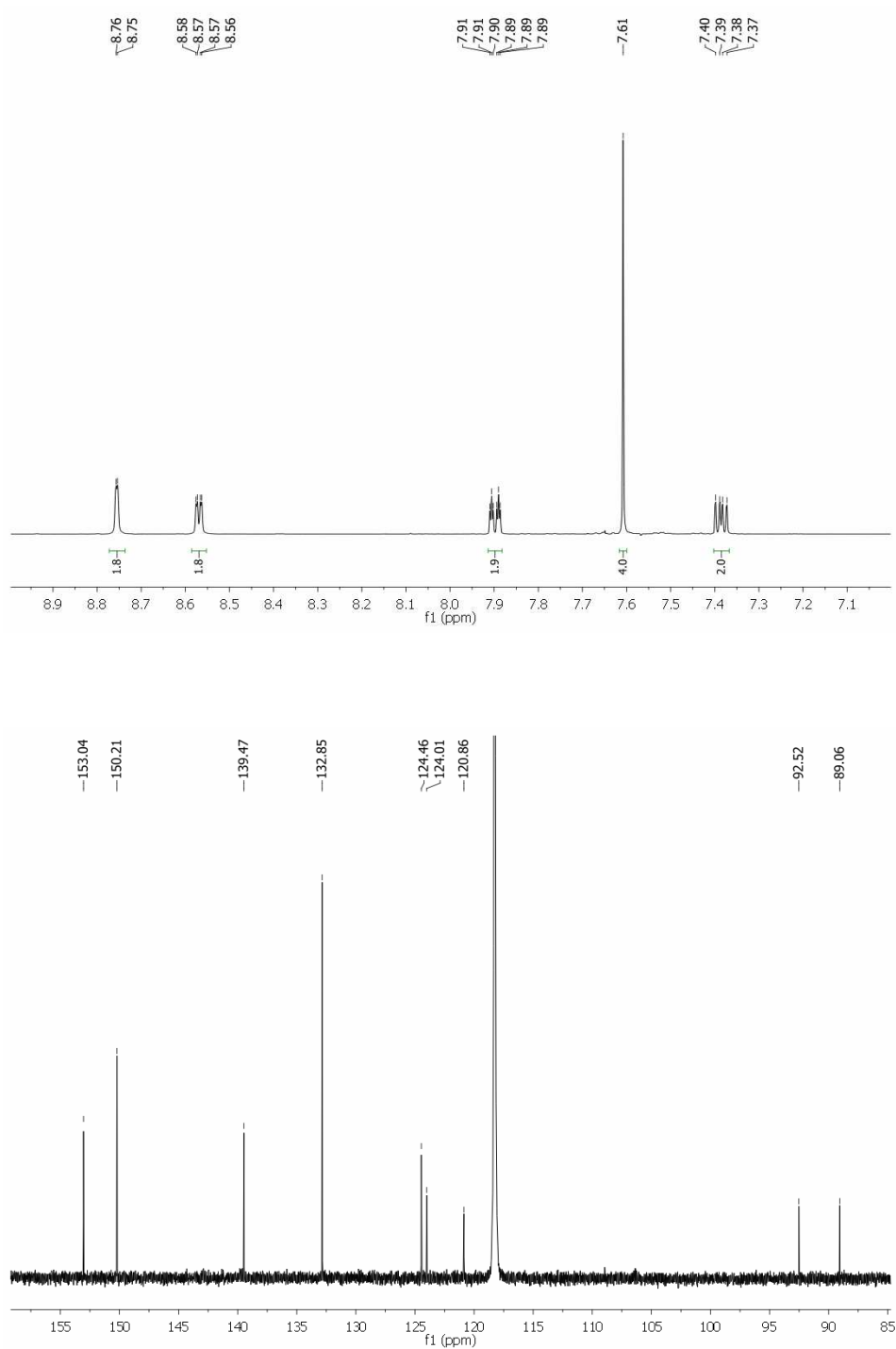


Figure S4: ¹H (top) and ¹³C (bottom) NMR spectra (CD₃CN) of L₂

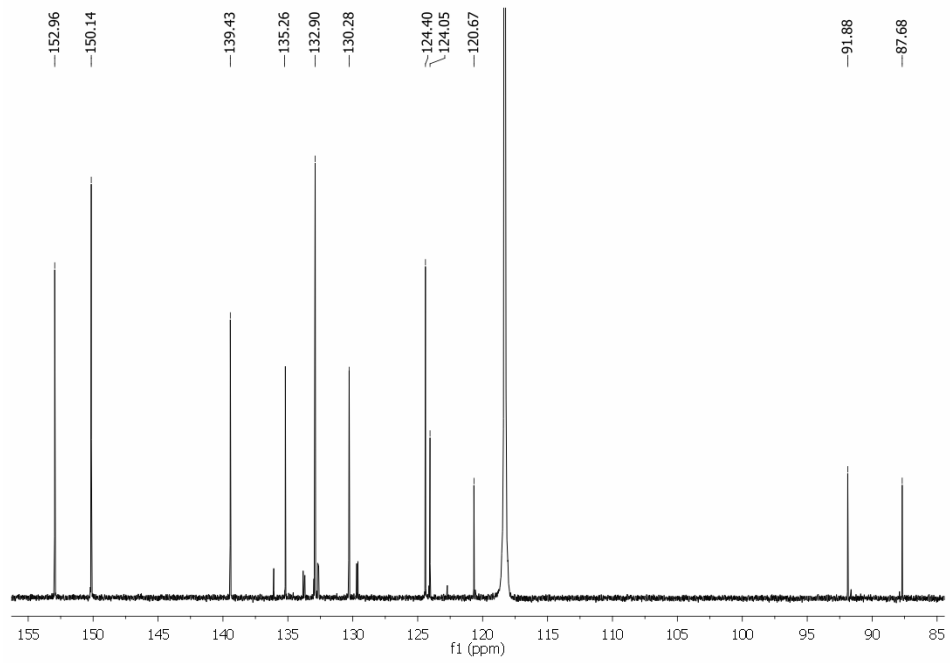
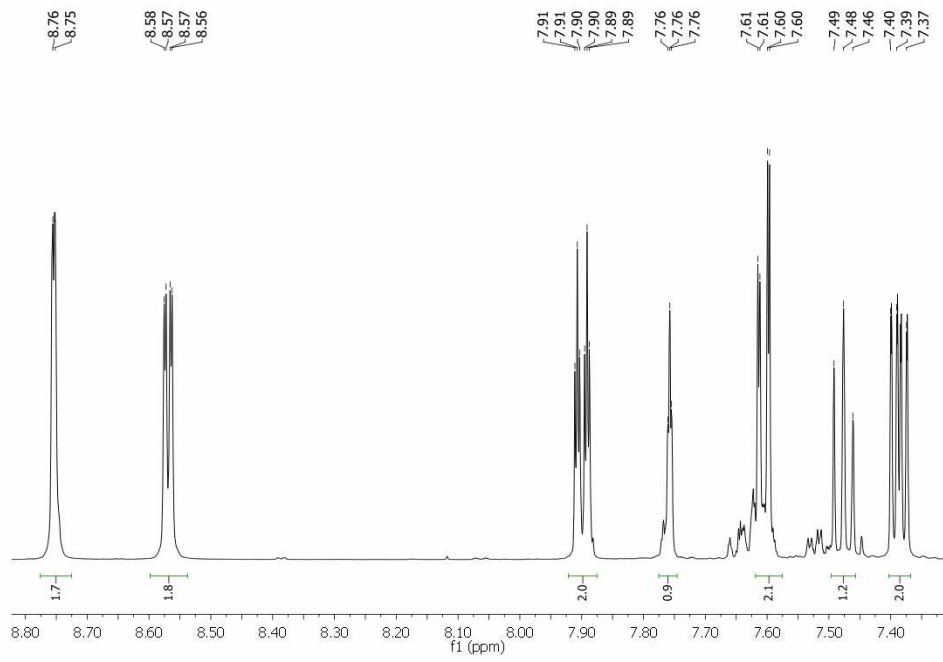


Figure S5: ^1H (top) and ^{13}C (bottom) NMR spectra (CD₃CN) of **L₃**

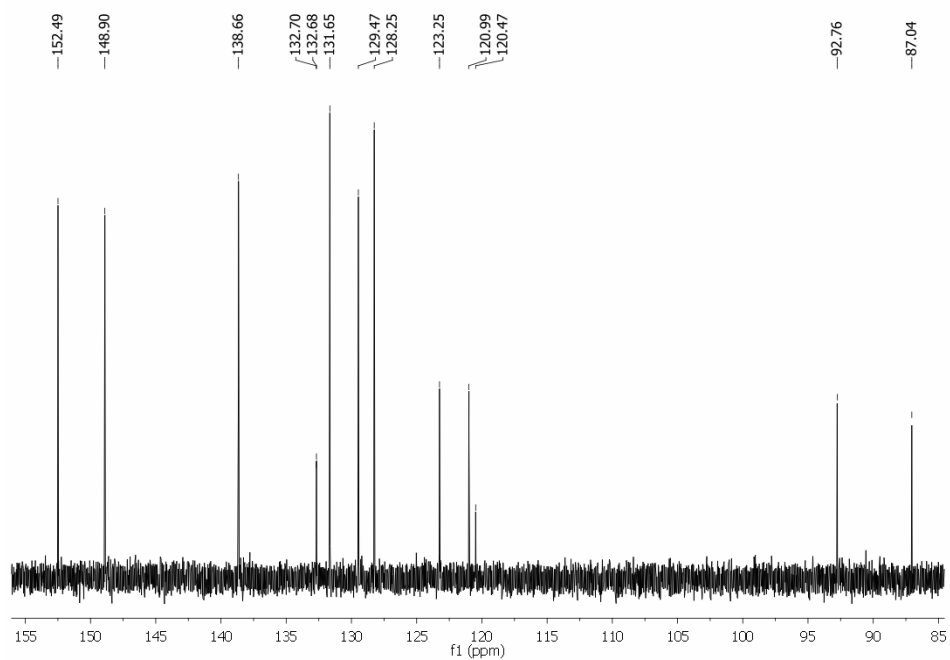
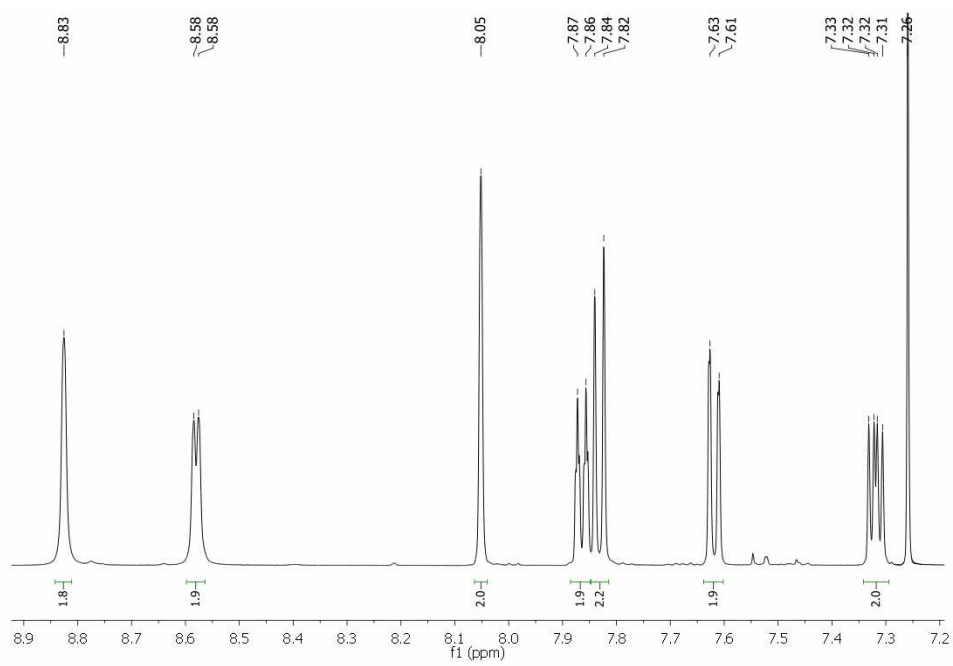


Figure S6: ^1H (top) and ^{13}C (bottom) NMR spectra (CDCl₃) of **L**₄

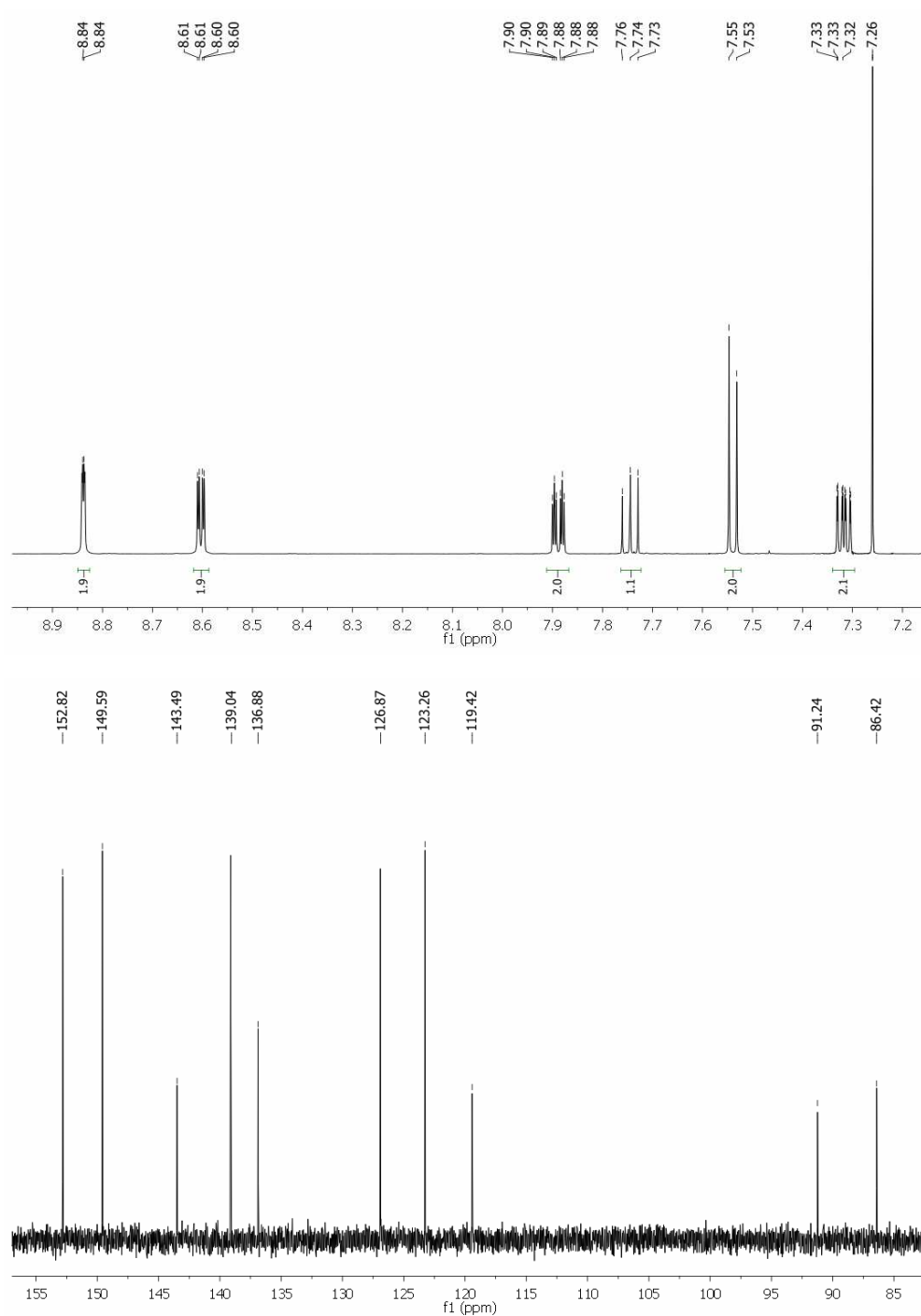


Figure S7: ^1H (top) and ^{13}C (bottom) NMR spectra (CDCl_3) of **L5**

3. Selected HR-ESI Mass Spectra of the Gold(I) complexes.

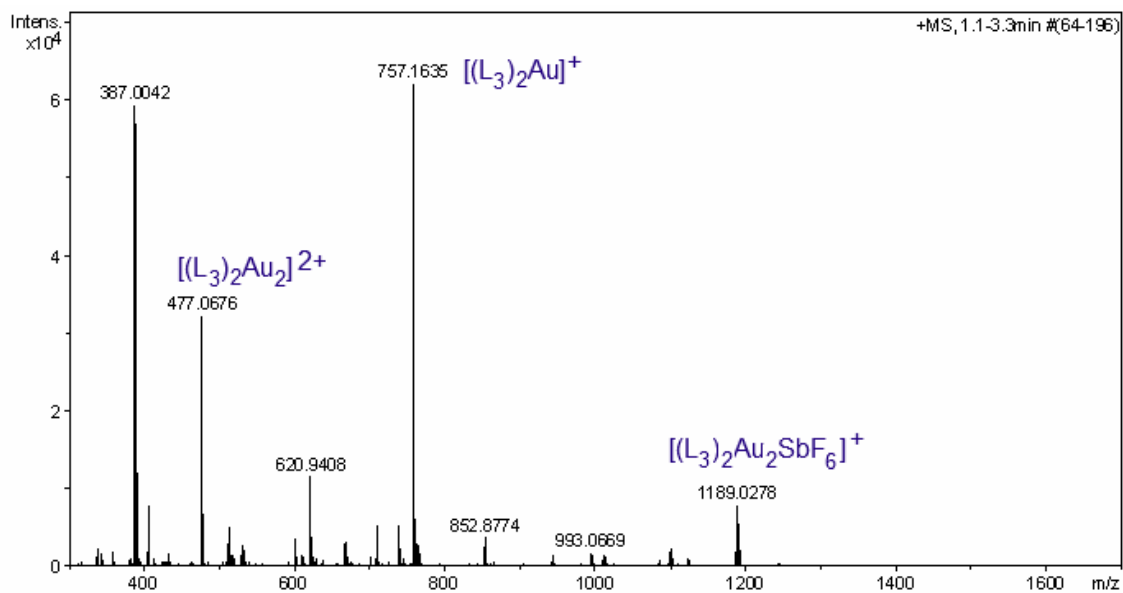


Figure S8: HR-ESI Mass Spectrum (+ve ion, MeCN) of $[(L_3)_2Au_2](SbF_6)_2$.

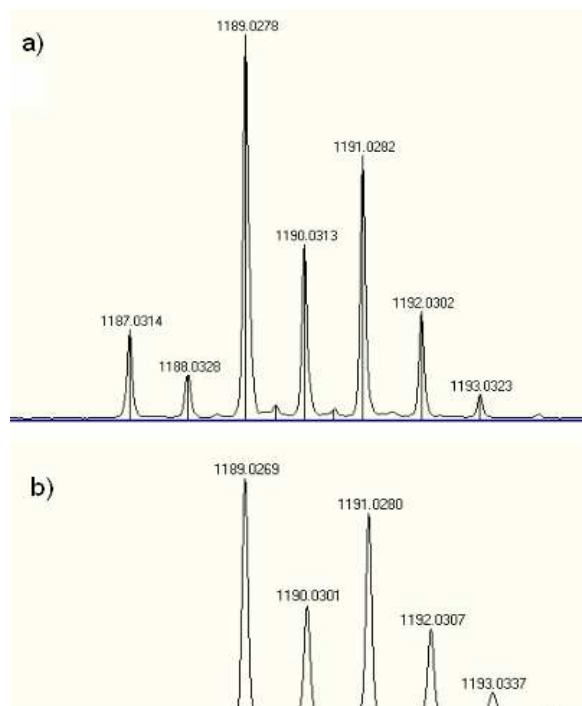


Figure S9: a) experimental and b) theoretical isotope patterns for $[(L_3)_2Au_2SbF_6]^+$

4. Selected NMR Spectra and Stacked Plots of the Ag(I) complexes

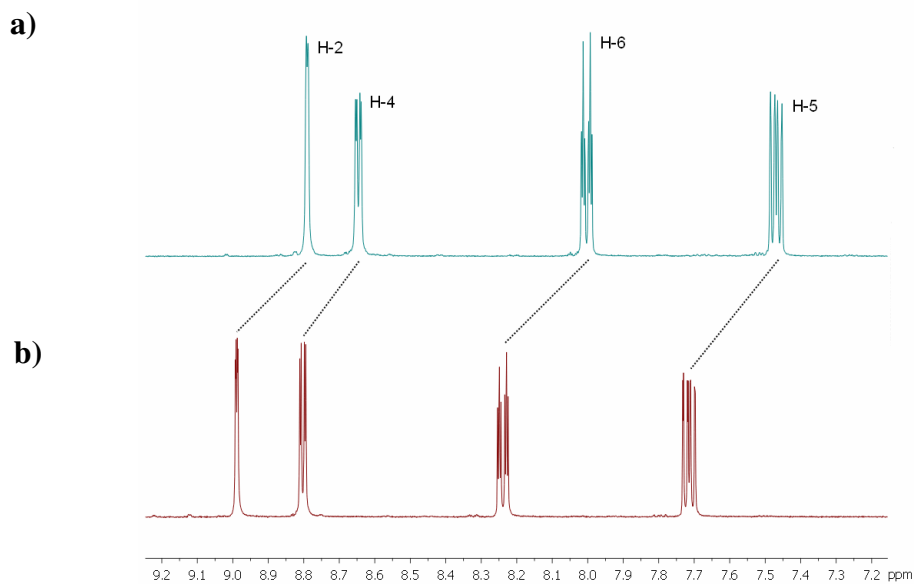


Figure S10: Stacked ^1H NMR spectra (d_6 -acetone) of a) L_1 and b) $\{[(\text{L}_1\text{Ag})](\text{SbF}_6)\}_n$

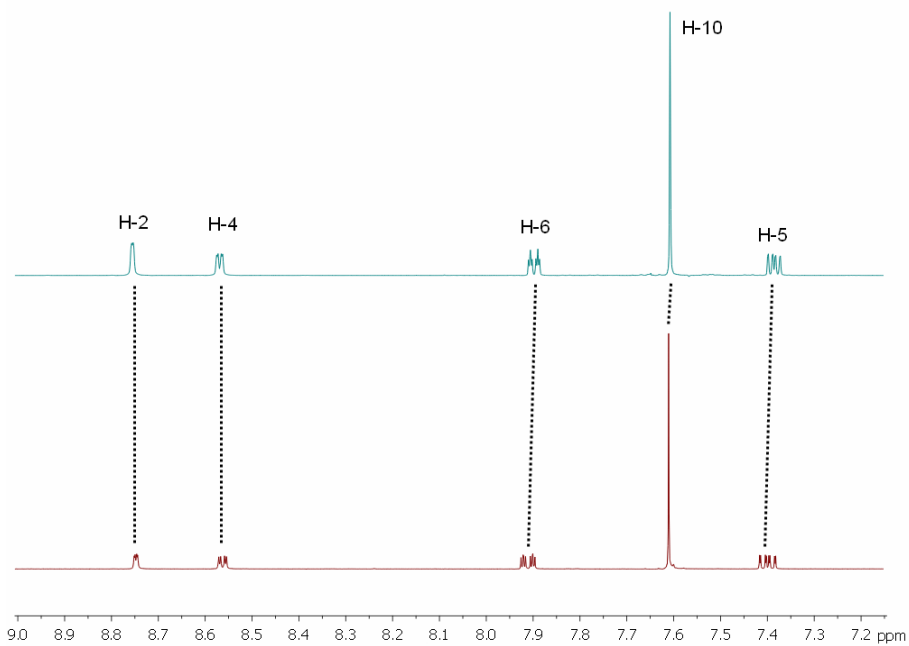


Figure S11: Stacked ^1H NMR spectra (CD_3CN) of a) L_2 and b) $\{[(\text{L}_2\text{Ag})](\text{SbF}_6)\}_n$

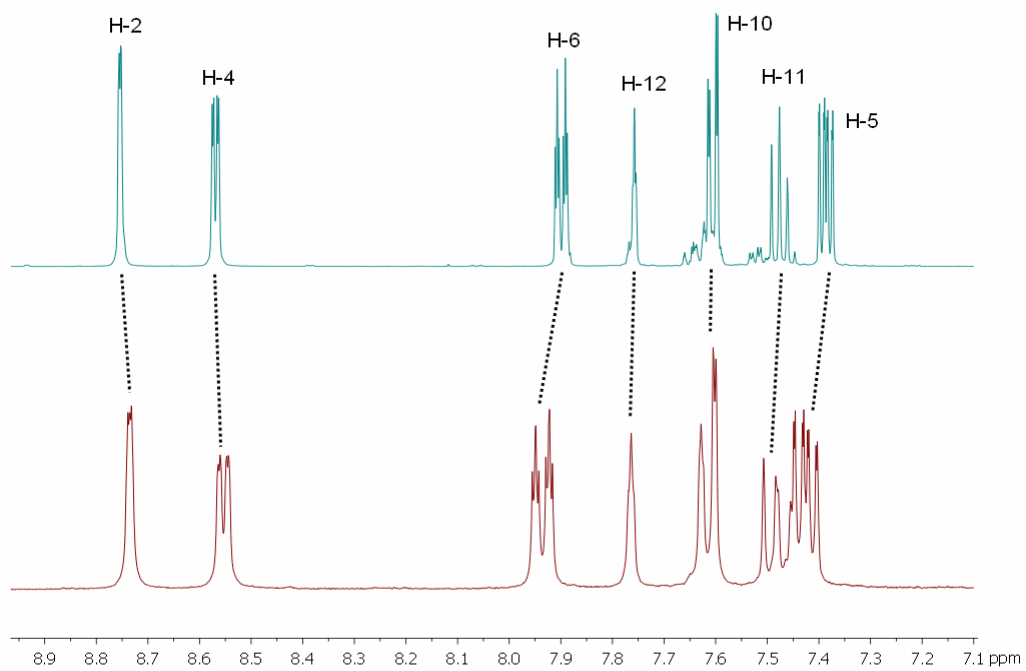


Figure S12: Stacked ¹H NMR spectra (CD₃CN) of a) **L**₃ and b) **[L**₃Ag]₂(SbF₆)₂

5. Selected HR-ESI Mass Spectra of the Ag(I) complexes

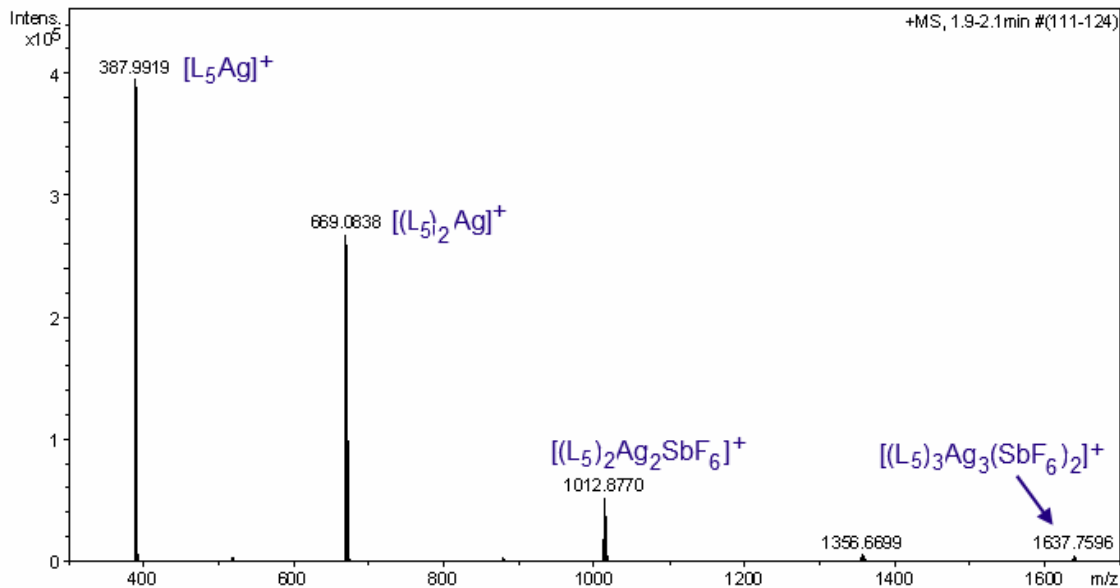


Figure S13: HR-ESI Mass Spectrum (+ve ion, MeCN) of $[(L_5)_2Ag_2](SbF_6)_2$.

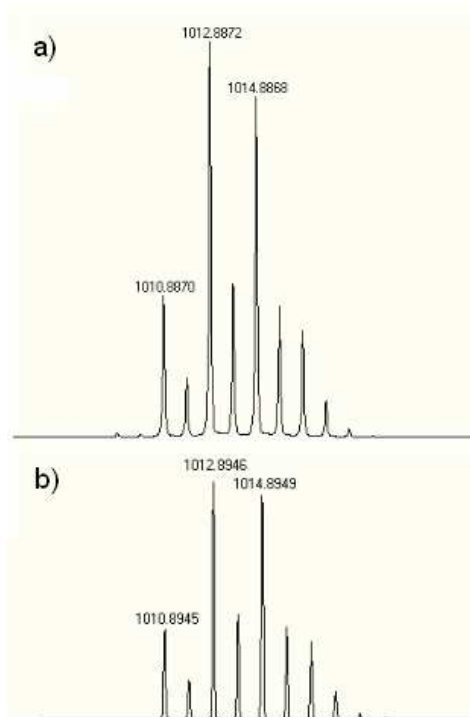


Figure S14: a) experimental and b) theoretical isotope patterns for $[(L_5)_2Ag_2SbF_6]^+$

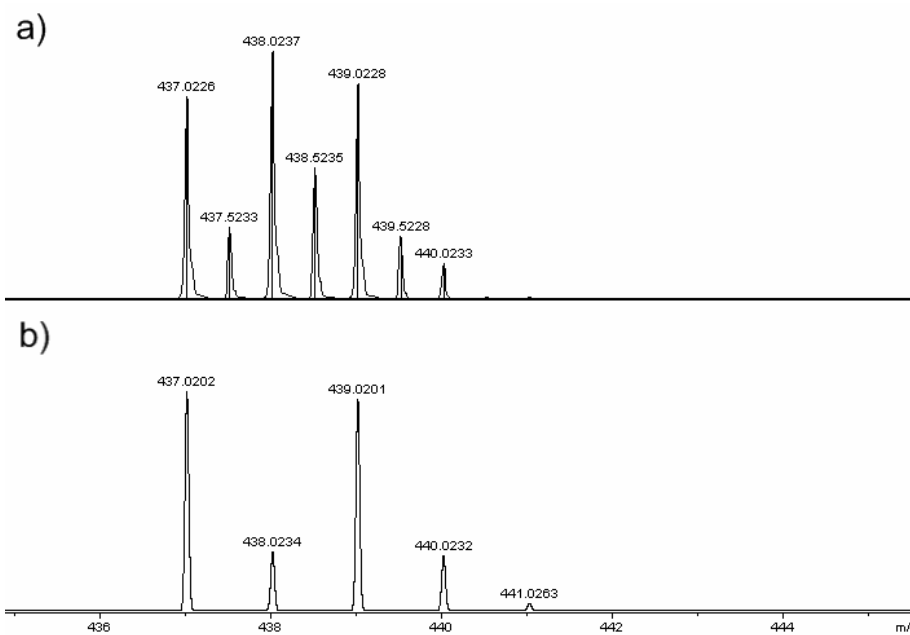


Figure S15: a) experimental and b) theoretical isotope patterns for $[(L_4)Ag]^+$ ion from a CH_3CN solution of $[(L_4)_2Ag_2](BF_4)_2$.

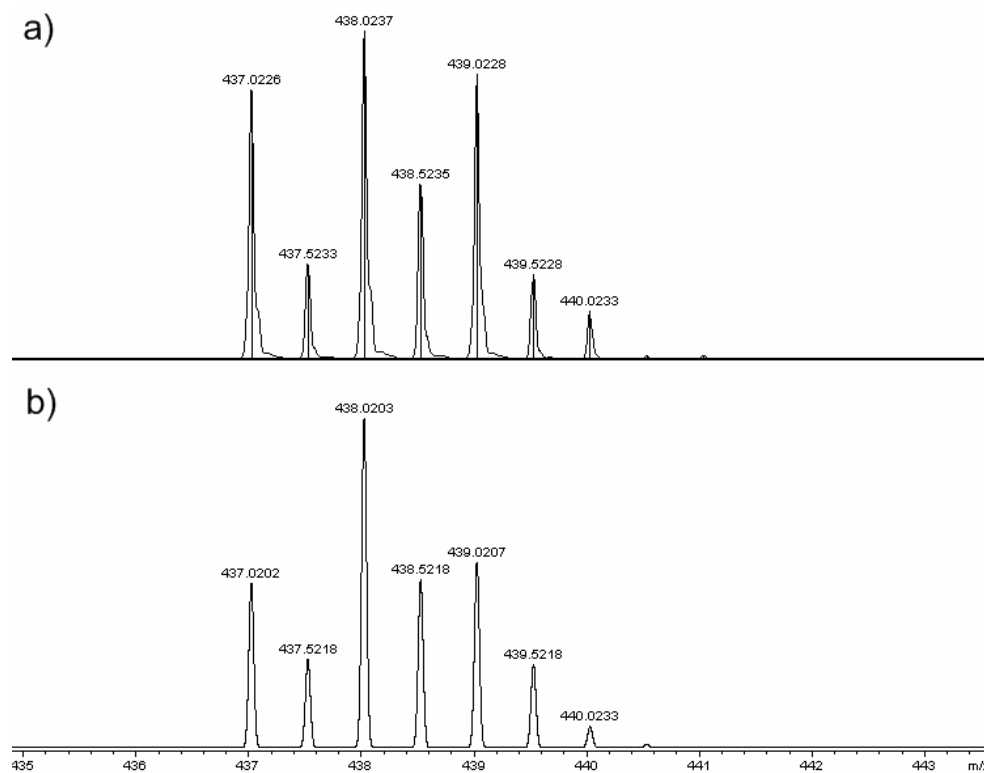


Figure S16: a) experimental and b) theoretical isotope patterns for $[(L_4)_2Ag_2]^{2+}$ ion from a CH_3CN solution of $[(L_4)_2Ag_2](BF_4)_2$.

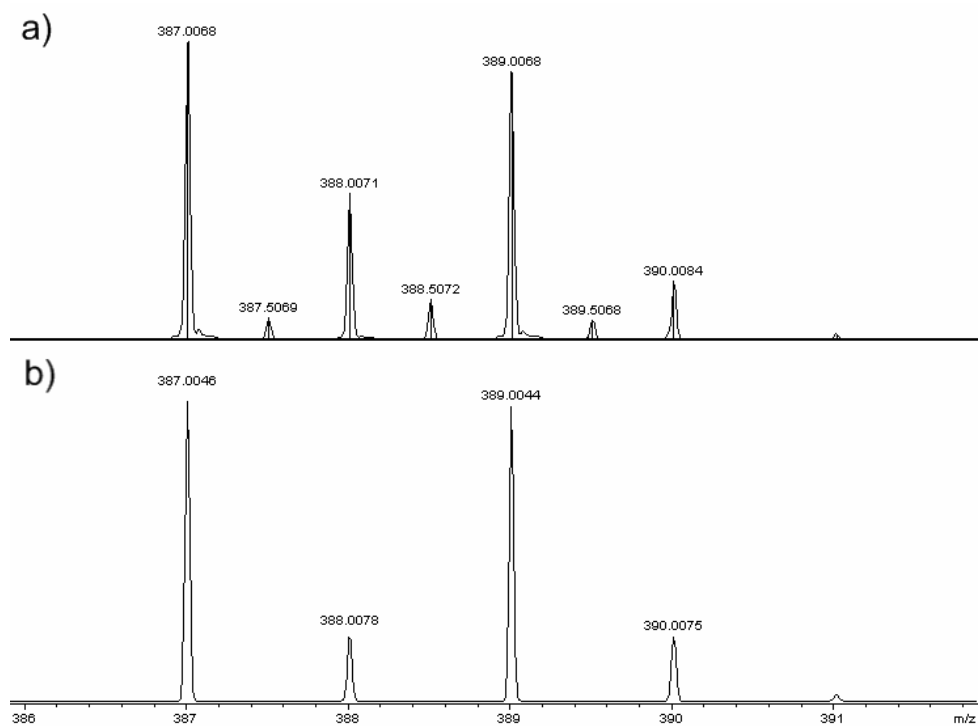


Figure S17: a) experimental and b) theoretical isotope patterns for $[(L_3)Ag]^+$ ion from a CH_3CN solution of $[(L_3)_2Ag_2](ClO_4)_2$.

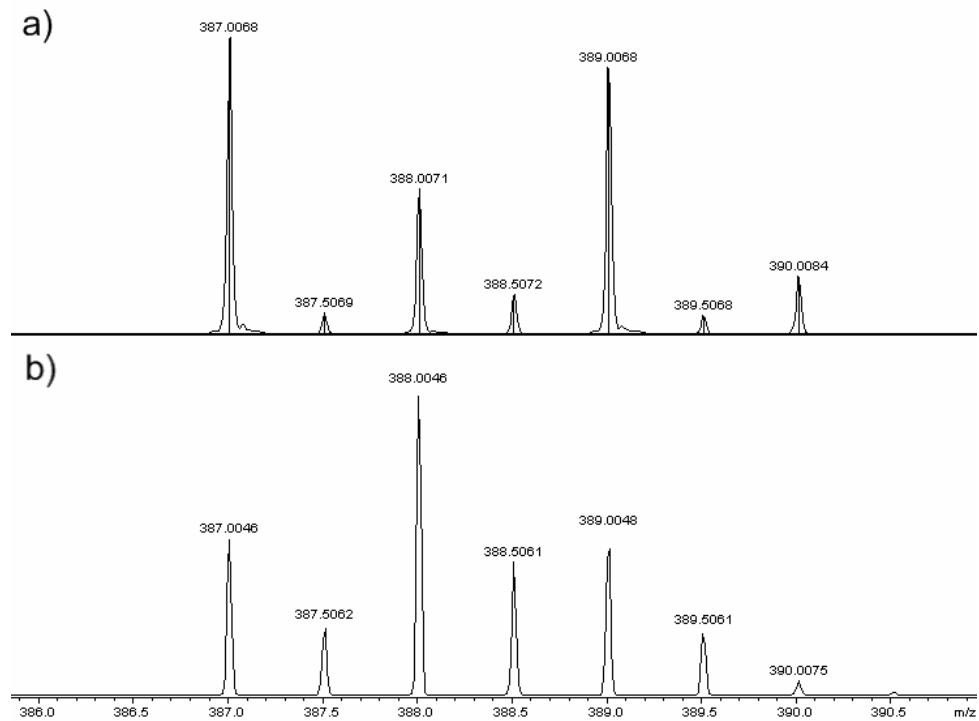


Figure S18: a) experimental and b) theoretical isotope patterns for $[(L_3)_2Ag_2]^{2+}$ ion from a CH_3CN solution of $[(L_3)_2Ag_2](ClO_4)_2$.

6. Proposed Structures of the metallomacrocycles

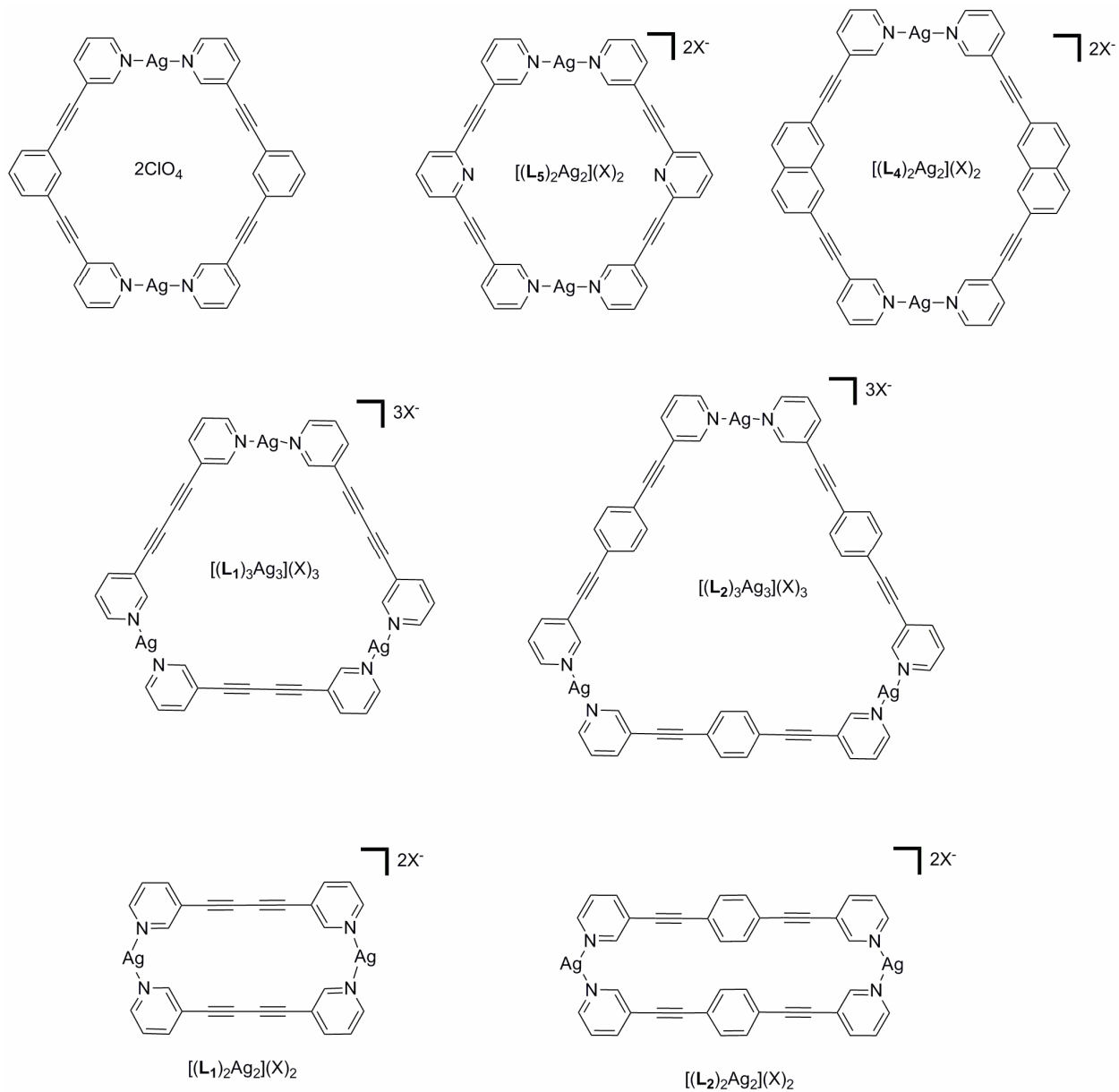


Figure S19. Proposed structures of the metallomacrocycles.

7. X-Ray Crystallography

7.1 Packing Diagrams for $[(L_3)_2Ag_2](ClO_4)_2 \cdot 3H_2O$.

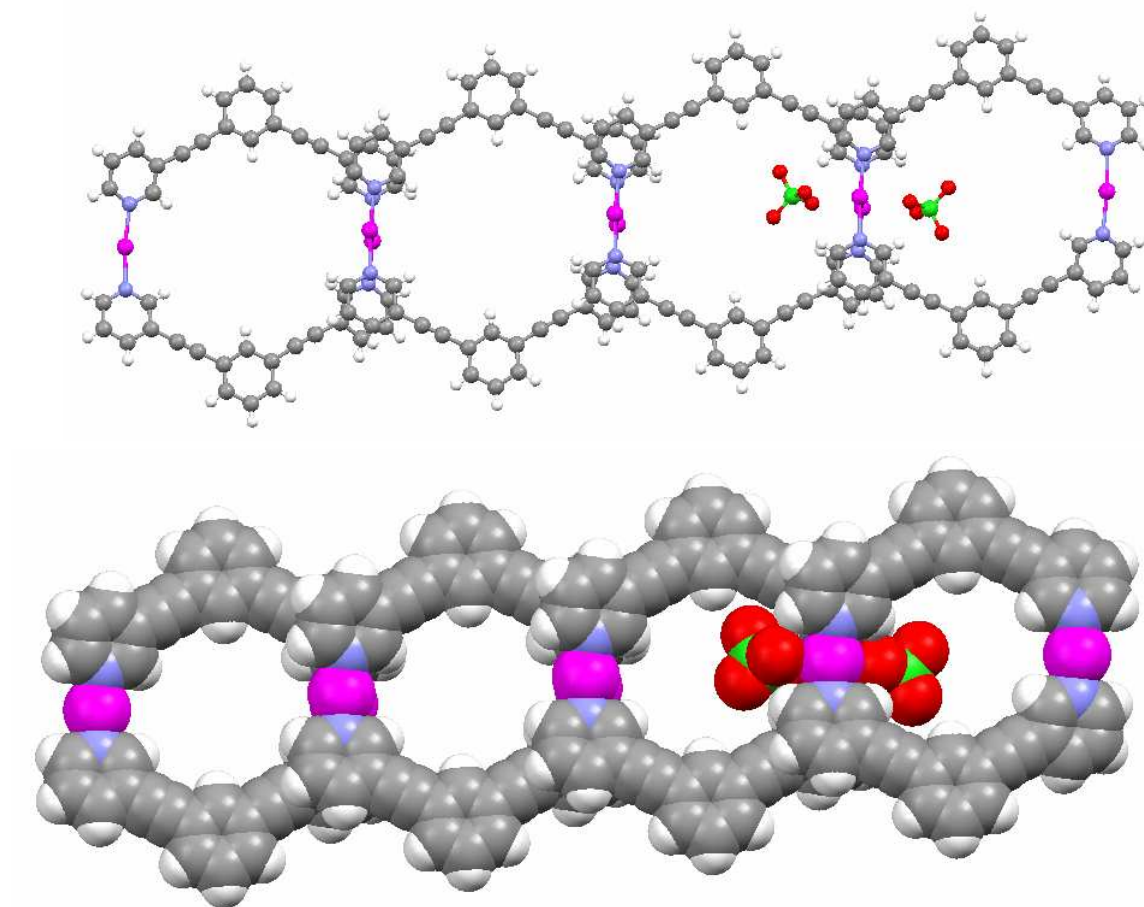


Figure S20: Ball-and-stick and space-filling molecular diagrams of the structure of $[(L_3)_2Ag_2](ClO_4)_2 \cdot 3H_2O$ showing the position of the ClO_4^- counter anions.

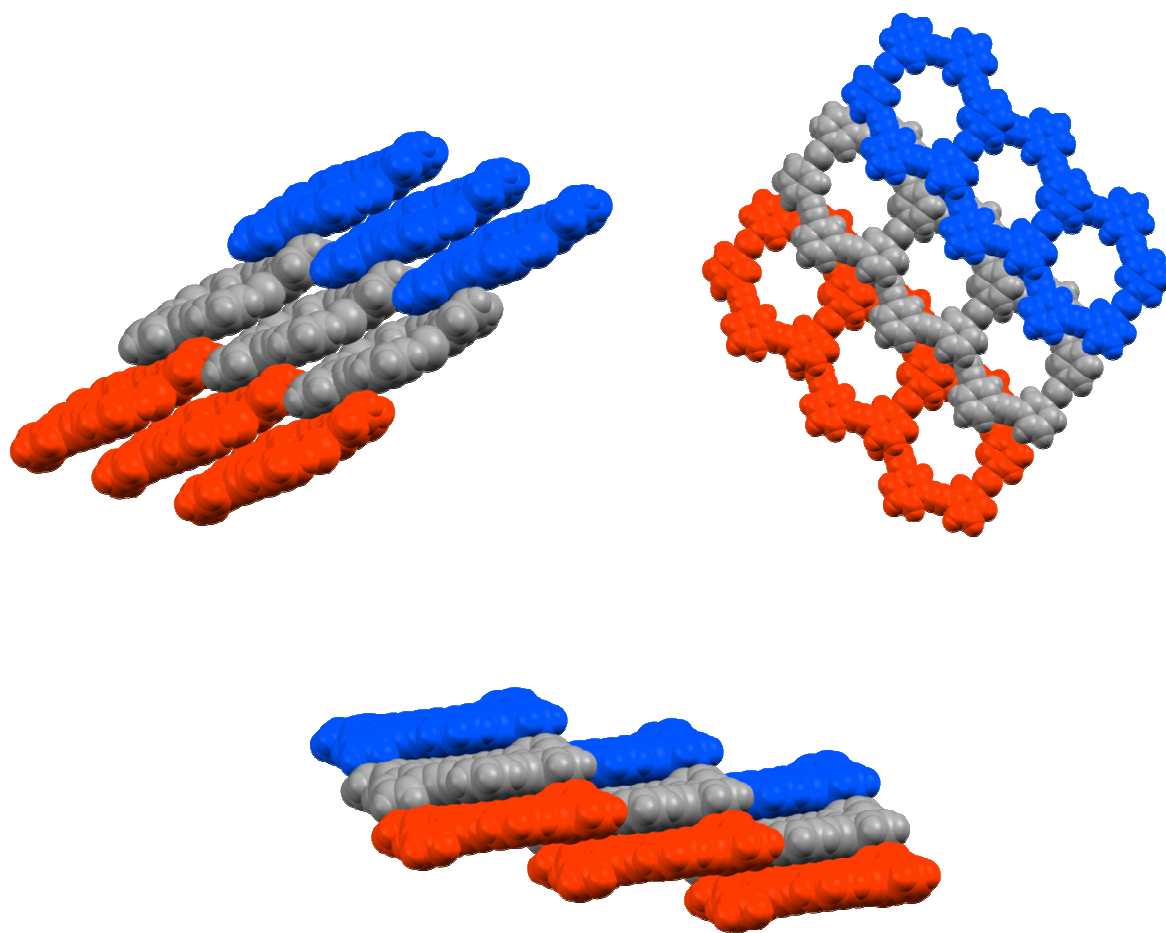


Figure S21: Space-filling molecular diagrams of $[(L_3)_2Ag_2](ClO_4)_2 \cdot 3H_2O$ showing interdigitation of the step-wise layers. For clarity, individual layers are shown in different colors.

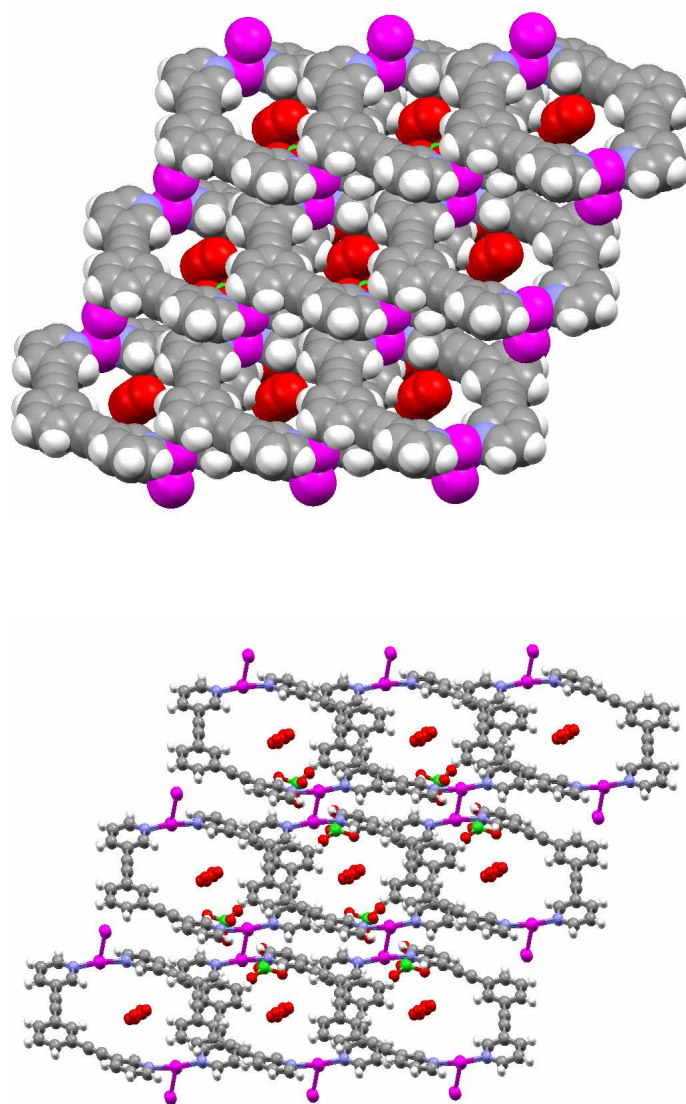


Figure S22: Ball-and-stick and space-filling molecular diagrams of the structure of $[(\mathbf{L}_3)_2\text{Ag}_2](\text{ClO}_4)_2 \cdot 3\text{H}_2\text{O}$ showing the position of the disordered H_2O within the nanotubes

7.2 Packing Diagrams for $\{[\text{L}_5\text{Ag}](\text{ClO}_4)\bullet\text{Et}_2\text{O}\}_n$.

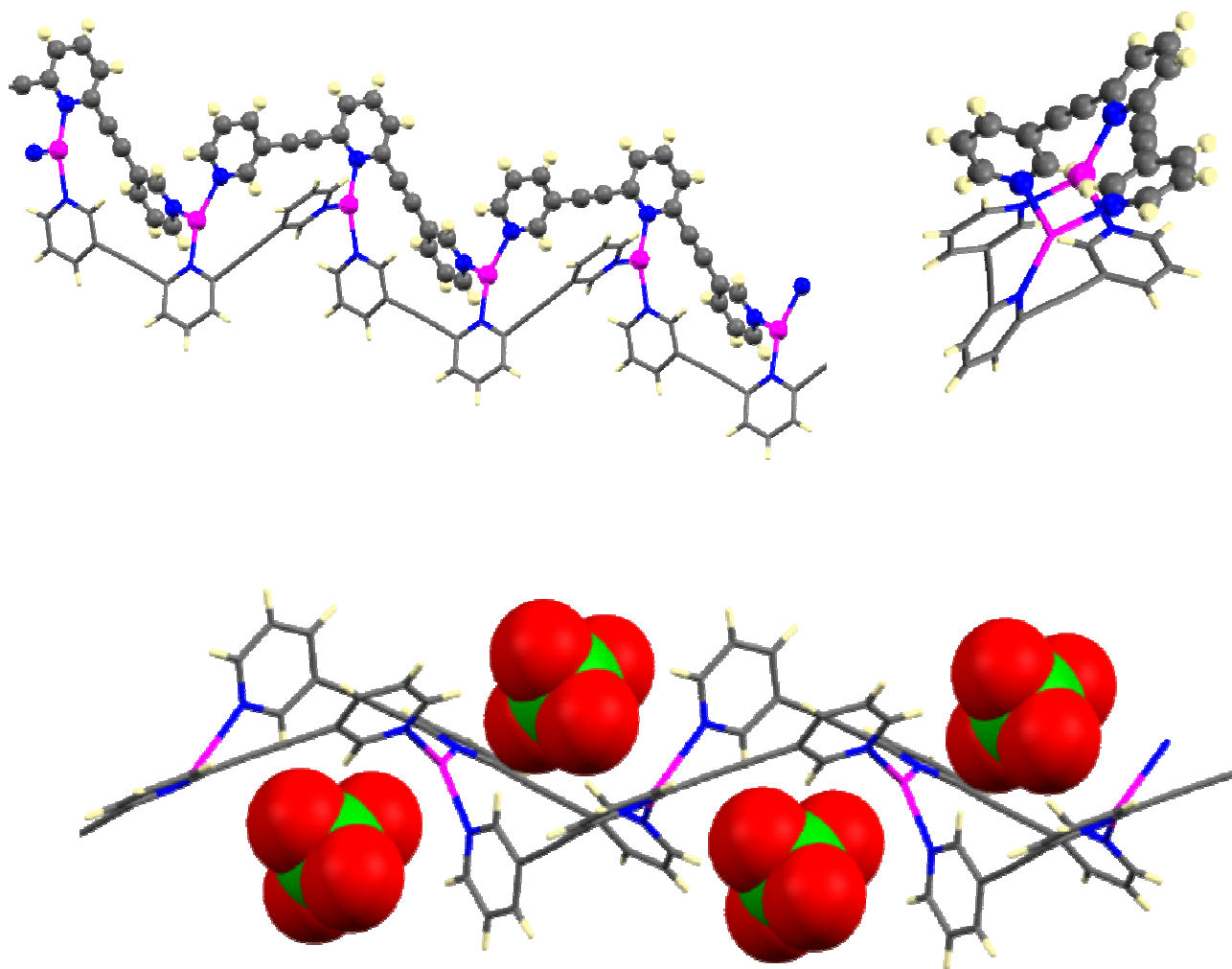


Figure S23: Three representations of the polymeric structure of $\{[\text{L}_5\text{Ag}](\text{ClO}_4)\bullet 0.5\text{Et}_2\text{O}\}_n$. For clarity, individual layers are shown in different colors. Top, ball-and-stick and tube representations of the ladder polymer structure formed by $\{[\text{L}_5\text{Ag}](\text{ClO}_4)\bullet 0.5\text{Et}_2\text{O}\}_n$. The ClO_4^- anions and diethyl ether molecules have been omitted for clarity. Bottom, a tube representation of the ladder polymer structure of $\{[\text{L}_5\text{Ag}](\text{ClO}_4)\bullet 0.5\text{Et}_2\text{O}\}_n$ showing the position of ClO_4^- anions.

7.3 Packing Diagrams for $\{[\mathbf{L}_3\text{Ag}](\text{SbF}_6)_2\}_n$.

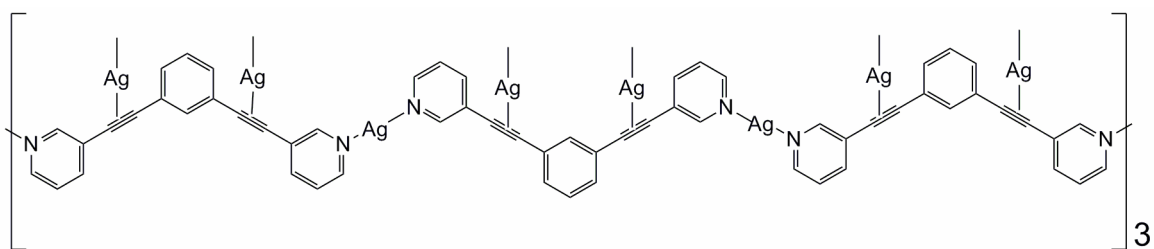


Figure S24: Chemdraw structure of the disordered twined coordination polymer $\{[\mathbf{L}_3\text{Ag}](\text{SbF}_6)\}_n$. In the crystal three disordered polymer strands are held together by additional Ag(I) ions that bond to the \mathbf{L}_3 ligands alkyne units. Despite the disorder in the X-ray structure it clearly indicates that the anion plays an important role in the formation of the final solid state structure. When the ClO_4^- counter ion is used the macrocyclic structure is maintained in the solid state. However, changing the counter ion to SbF_6^- generates a ring opened disordered polymeric structure in the solid state.

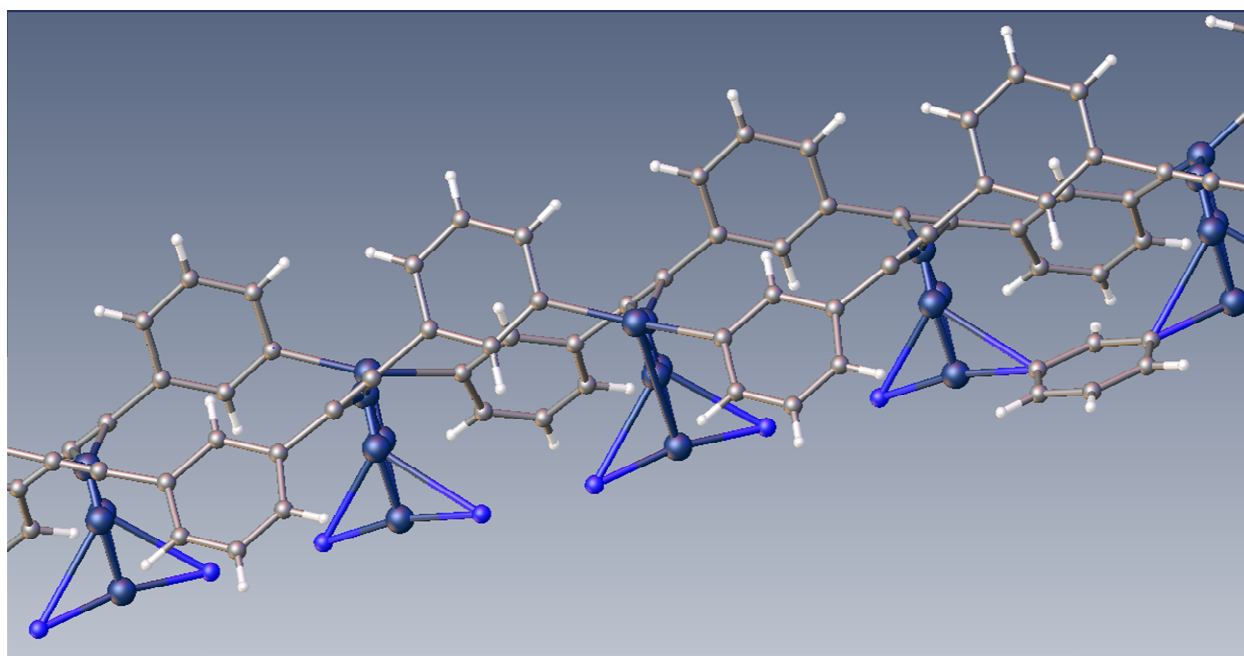


Figure S25: A ball and stick representation of the structure of the disordered twined coordination polymer $\{[\mathbf{L}_3\text{Ag}](\text{SbF}_6)\}_n$.

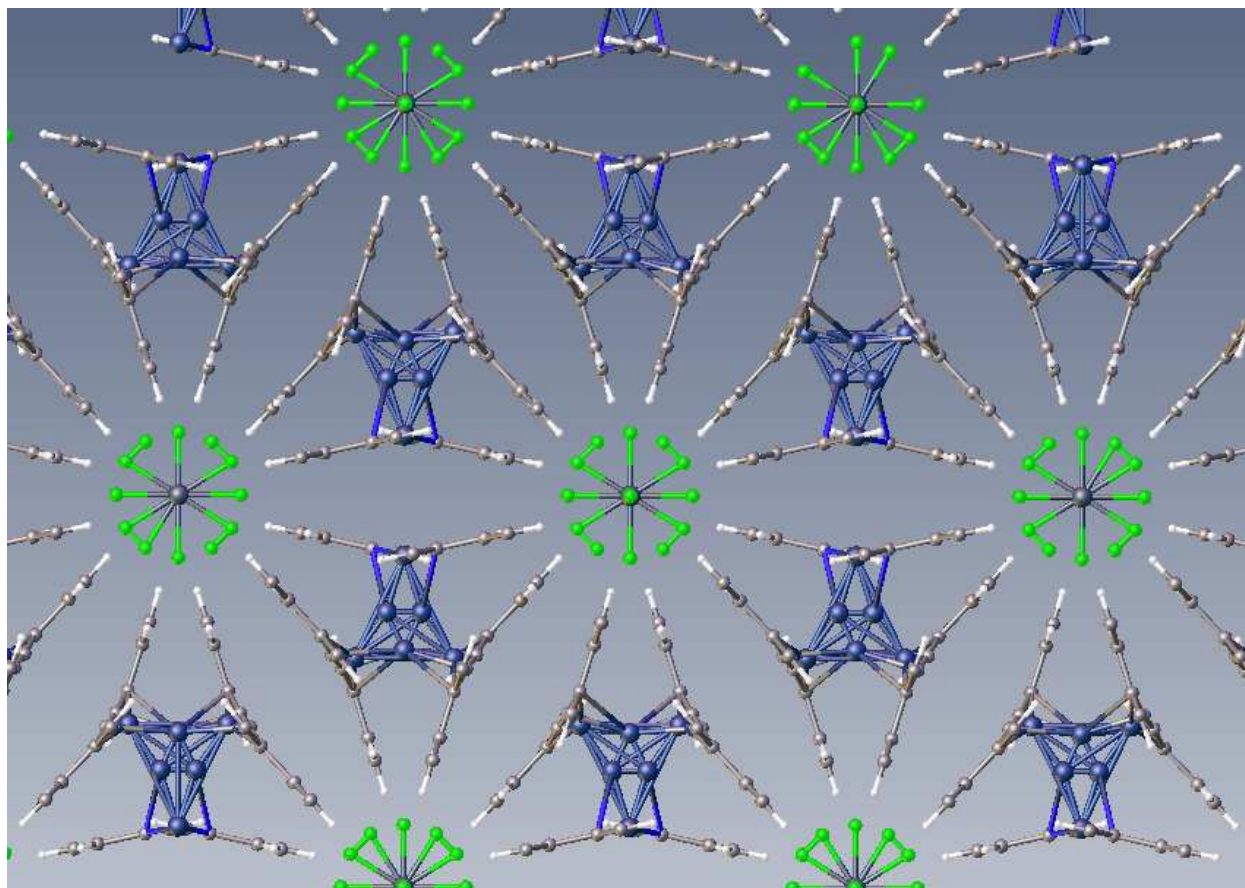


Figure S26: A ball and stick representation showing the high symmetry of the disordered twinned coordination polymer $\{[L_3Ag](SbF_6)\}_n$. Three independent polymer strands are held in close proximity by alkyne bonded disordered Ag^+ ions.

8. X-ray Crystallographic Data

8.1 X-ray data collection and refinement

X-ray data for $\{[L_3Ag](SbF_6)\}_n$ were collected at 123 K on a Rigaku Spider diffractometer equipped with a copper rotating anode X-ray source and a curved image plate detector. Structures were solved by direct methods, and refined against F^2 using anisotropic thermal displacement parameters for all non-hydrogen atoms. Hydrogen atoms were placed in calculated positions and refined using a riding model (except where noted below).

Using XPREP, the data merged poorly ($R(\text{int}) = 0.18$) into the obvious primitive trigonal/hexagonal cell. Data merged satisfactorily ($R(\text{int}) = 0.074$) into monoclinic P or equivalent C lattice, or into an orthorhombic C-centered lattice. A satisfactory solution could only be extracted in space group *Cccm*. An SbF_6 anion with badly disordered F atoms sits on a special position ($2/m$ symmetry) leading to a total of four SbF_6 per unit cell, and hence to a total count of four Ag^+ ions per cell. The expected bis-alkyne moiety (py \equiv Ph \equiv py, where \equiv denotes the alkyne bond, Ph a bis-meta-substituted phenyl group and py a meta-substituted pyridyl group) was not to be found (in this or any other space group attempted including C1). Rather, the structure is comprised of an apparently oligomeric alkyne and stacked but disordered pyridyl groups. Pairs of pyridyl groups are bridged by substoichiometric amounts of Ag^+ ions (total 2 per cell), giving linear N-Ag-N moieties. Pairs of apparent alkyne oligomers are bridged by substoichiometric amounts of Ag^+ ions to give linear bis-alkyne Ag moieties; and an alkyne chain is bridged to the pyridyl chain through by substoichiometric amounts of Ag^+ ions. Application of space-group symmetry operations creates linear zig-zag chains of the pyridyl-Ag moieties and of apparently oligomeric alkyne-phenyl groups. However, a fourth crystallographically distinct Ag^+ sits

essentially between the two alkyne carbon atoms. Initial models focussed on polymeric alkynyl-phenyl chain with pyridyl groups as polymer chain terminators.

However, as there was little chemical evidence of polymerisation having taken place, we turned to a model wherein the py-≡-Ph-≡-py units are disordered by $\pm 1/3$, noting that the PyN..Npy separation was essentially identical to the distance spanned by the ≡- moiety and the 120 deg angles created by meta substitution. Accordingly, with respect to the py-≡-Ph-≡-py moiety, each aromatic ring is $2/3$ pyridyl and $1/3$ phenyl. This leaves the alkynyl group with occupancy of $2/3$ and the two crystallographically independent nitrogen sites in this moiety with an occupancy of $1/6$. The asymmetric unit comprises an alkynyl moiety and two half rings sitting perpendicular to crystallographic mirror planes with two of the substoichiometric silver ions in general positions [one coordinated linearly by a pair of pyridyl nitrogens, present in $1/48$ of full occupancy ($1/3$ per cell) and the other associated asymmetrically with alkynyl groups and the separate pyridyl group, present in $1/24$ of full occupancy ($2/3$ per cell)] and the third Ag^+ sitting on a two-fold axis [bridging linearly two alkynyl groups, present in $1/8$ of full occupancy (1 Ag^+ per cell)]. Completing the asymmetric unit, the separate pyridyl rings have crystallographically imposed mirror symmetry about a plane perpendicular to the molecular plane and the substoichiometric Ag^+ ion sits on a two-fold axis with $1/4$ of full site occupancy (2 per cell). Thus, the composition of the unit cell is non-stoichiometric. The structure is also significantly twinned with hexagonal twin law $(0.5 \ 0.5 \ 0 / \ 1.5 \ -0.5 \ 0 / \ 0 \ 0 \ 1)$ yielding a final twin component of $0.130(12)$.

Table S1: Crystallographic data for $\{[\mathbf{L}_3\text{Ag}](\text{SbF}_6)\}_n$.

Compound	$\{[\mathbf{L}_3\text{Ag}](\text{SbF}_6)\}_n$
Formula	$\text{C}_{14}\text{H}_9\text{F}_{12}\text{SbAg}_4\text{N}_3$
Formula weight	1741.78
Crystal system	Orthorhombic
Space group	<i>Cccm</i>
a , Å	12.9114(17)
b , Å	22.3632(17)
c , Å	11.9153(8)
α , °	90.
β , °	90.
γ , °	90.
V , Å ³	3440.4(6)
Z	2
Cryst. size, color, habit	0.35 x 0.21 x 0.17 mm, pale yellow , block
ρ_{calc} , mg/mm ³	1.681
μ , mm ⁻¹	11.359
Reflections collected	22241
Independent reflections (R_{int})	1542[$R(\text{int}) = 0.1053$]
Data/restraints/parameters	1542/150/178
Goodness-of-fit on F^2	1.020
Final R_1 and wR_2 indexes [$I > 2\sigma(I)$]	$R_1 = 0.0635$, $wR_2 = 0.1800$
Final R_1 and wR_2 indexes [all data]	$R_1 = 0.0740$, $wR_2 = 0.1955$
Largest difference in peak and hole (eÅ ⁻³)	1.004 and -1.298
